JOURNAL OF GEOPHYSICAL RESEARCH: ATMOSPHERES, VOL. 118, 8054–8066, doi:10.1002/jgrd.50624, 2013

Direct top-down estimates of biomass burning CO emissions using TES and MOPITT versus bottom-up GFED inventory

Olga Pechony,[1] Drew T. Shindell,[1] and Greg Faluvegi[1]

Received 23 January 2013; revised 17 June 2013; accepted 3 July 2013; published 29 July 2013.

[1] In this study, we utilize near-simultaneous observations from two sets of multiple satellite sensors to segregate Tropospheric Emission Spectrometer (TES) and Measurements of Pollution in the Troposphere (MOPITT) CO observations over active fire sources from those made over clear background. Hence, we obtain direct estimates of biomass burning CO emissions without invoking inverse modeling as in traditional top-down methods. We find considerable differences between Global Fire Emissions Database (GFED) versions 2.1 and 3.1 and satellite-based emission estimates in many regions. Both inventories appear to greatly underestimate South and Southeast Asia emissions, for example. On global scales, however, CO emissions in both inventories and in the MOPITT-based analysis agree reasonably well, with the largest bias (30%) found in the Northern Hemisphere spring. In the Southern Hemisphere, there is a one-month shift between the GFED and MOPITT-based fire emissions peak. Afternoon tropical fire emissions retrieved from TES are about two times higher than the morning MOPITT retrievals. This appears to be both a real difference due to the diurnal fire activity variations, and a bias due to the scarcity of TES data.

Citation: Pechony, O., D. T. Shindell, and G. Faluvegi (2013), Direct top-down estimates of biomass burning CO emissions using TES and MOPITT versus bottom-up GFED inventory, *J. Geophys. Res. Atmos.*, *118*, 8054–8066, doi:10.1002/jgrd.50624.

1. Introduction

[2] Scientists today enjoy an abundance of satellite, ground, and airborne observations providing plentiful information on the Earth's system, including its atmosphere and biosphere. Nevertheless, inferring comprehensive information on some processes remains a complicated task. One example is biomass burning emissions, which are of great importance in many research areas ranging from air quality to climate modeling.

[3] The most accurate and controlled way to measure fire emissions is in the laboratory, providing, however, only point information. Field measurements supply wider-scale data but still yield only local information and are mostly limited to prescribed fires. Towers offer the advantage of continuous observations but are too expensive and vulnerable to allow setting up a large-scale network. Aircraft provide regional-scale data, but observations are mostly limited to large plumes. Satellites gather consistent worldwide observations of atmospheric concentrations of species such as CO for which biomass burning is one of the largest emission sources. These observations still do not provide continuous global coverage but are rather a collection of snapshots that together make up a pseudoglobal data set.

[4] CO concentrations observed with satellites are a combination of local and nonlocal sources with variable relative influence. Traditional techniques for "top-down" emission estimates from satellite data aim to disentangle those influences by relying on interpretation using chemistry transport models (CTMs) and inverse modeling [e.g., *Jones et al.*, 2003; *Müller and Stavrakou*, 2005; *Kopacz et al.*, 2010; *Gonzi et al.*, 2011; *Hooghiemstra et al.*, 2012]. This technique generally requires the assumption that model biases are mostly due to differences in biomass burning inventories. However, inaccuracies in the models, particularly the representation of convective transport, can lead to significant uncertainties in CO emission estimates on global, and especially on regional, scales [*Tost et al.*, 2010; *Jiang et al.*, 2011, 2013]. The OH distribution in the model can also significantly influence the inversion results [*Kopacz et al.*, 2010; *Hooghiemstra et al.*, 2011; *Jiang et al.*, 2011]. *Jiang et al.* [2011] note that even using the same satellite observations for the same period, estimates of south Asian emissions of *Stavrakou and Müller* [2006] and *Arellano et al.* [2004] differed by 75%. Discrepancies of the same order were found by *Heald et al.* [2004] when comparing previous emission estimates for this region. Using the same version 3 of MOPITT data, *Jones et al.* [2009] and *Arellano and Hess* [2006] obtained significantly different CO estimates for the Southern Hemisphere, likely due to differences in the vertical transport in the models used in the inversions [*Jiang et al.*, 2013]. *Kopacz et al.* [2009] found that model resolution

[1]NASA Goddard Institute for Space Studies and Columbia Earth Institute, New York, New York USA.

Corresponding author: O. Pechony, NASA Goddard Institute for Space Studies, 2880 Broadway, New York, NY 10025, USA. (pechony@gmail.com)

2169-897X/13/10.1002/jgrd.50624

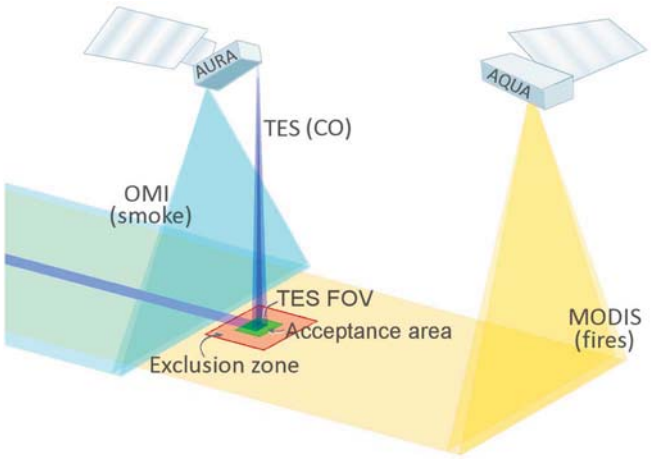

Figure 1. Illustration (not to scale) of the working scheme for the A-train sensors.

can also significantly affect emission estimates, leading to ~60% difference between results obtained with high- and low-resolution inversions for Japan and Korean peninsula.

[5] "Bottom-up" methods use satellite active fire observations to derive quantitative estimates of trace species emissions from biomass burning. The widely used "bottom-up" inventories Global Fire Emissions Database (GFED) version 2.1 (hereafter GFED2) [*van der Werf et al*., 2006] and GFED version 3.1 (hereafter GFED3) [*van der Werf et al*., 2010] are based on (1) burned areas derived either from Moderate Resolution Imaging Spectroradiometer (MODIS) fire pixel counts for GFED2 [*Giglio et al*., 2006] or coupling these with MODIS surface reflectance imagery for GFED3 [*Giglio et al*., 2009; *Giglio et al*., 2010], (2) fuel loads and combustion completeness factors from the satellite-constrained Carnegie-Ames-Stanford approach (CASA) biogeochemical model, and (3) a compilation of field and laboratory-based emission factors per dry matter burnt [*Andreae and Merlet*, 2001]. The GFED database is extensively used by the scientific community as prescribed or a priori fire emissions in global climate models (GCMs) and CTMs, as emission factors (per MODIS fire count or burned area) in fire models, and as a reference for evaluating modeling results [e.g., *Pechony and Shindell*, 2009; *Kopacz et al*., 2010; *Li et al*., 2012]. However, there are substantial uncertainties in the burned area estimates, fuel loads, and combustion completeness used in GFED [*van der Werf et al*., 2006]. Considerable differences are often found between the "bottom-up" and the "top-down" emission estimate [e.g., *Arellano et al*., 2004; *Bian et al*., 2007; *Kopacz et al*., 2010; *Bond et al*., 2013]. The *Arellano et al*. [2004] top-down inversion results for East Asia were about a factor of 2 higher than the bottom-up estimates. *Bian et al*. [2007] compared four bottom-up and two top-down inventories, finding agreement in global annual emissions within 30% but large regional discrepancies of up to a factor of 5. Top-down estimates in *Kopacz et al*. [2010] were 60% higher than bottom-up inventories, with especially large differences in comparison with tropical biomass burning in the GFED2 inventory.

[6] Considering the significant impact of model biases on the top-down estimates obtained using inversion analysis [*Tost et al*., 2010; *Hooghiemstra et al*., 2011; *Jiang et al*., 2011, 2013], we suggest here an approach different from the traditional top-down methods, avoiding inversion modeling. Utilizing the advantage of near-simultaneous observations from multiple satellite sensors, we discriminate between clear background and fire-related satellite CO retrievals, eliminating the need for inverse modeling to determine what portion of observed amounts originated in fires. We obtain vertically resolved observations of fire-related CO from the Tropospheric Emission Spectrometer (TES) and Measurements of Pollution in the Troposphere (MOPITT) satellite sensors and compare them with CO simulated within the NASA Goddard Institute for Space Studies (GISS) GCM Model-E2 using fire emissions prescribed from the GFED2 and GFED3 databases. We also derive CO emissions rates per MODIS fire count, which can be directly compared to GFED2 and GFED3 emission rates.

2. Method and Instruments

[7] Satellites of the A-train constellation, passing the equator in the local afternoon, observe various atmospheric and land parameters. With the closing Aura spacecraft lagging the lead Aqua satellite by 15 min, we can regard these observations as near simultaneous. We segregate vertically resolved CO observations collected with the TES instrument onboard Aura (level 2 version F05 nadir product) into two major categories. The “fire” category is assigned whenever the MODIS sensor onboard the Aqua satellite records active fire pixels in the $0.2° \times 0.2°$ “acceptance” area surrounding TES field of view (FOV, $\sim 5.3 \times 8.3$ km^2). The “background” category is assigned when there are no fire pixels recorded by MODIS and no biomass burning smoke aerosols are detected by the Ozone Monitoring Instrument (OMI) sensor (also on the Aura satellite) in the larger $1° \times 1°$ exclusion zone (see schematic illustration in Figure 1). Sensitivity testing showed that decreasing the size of the "acceptance" area reduces the amount of available TES data beyond usability. Increasing this region leads to a significant drop in fire-related CO concentrations, indicating a large number of CO retrievals not related to fire activity being misidentified as "fire".

[8] Sensors of the second ensemble used here are all onboard the Terra satellite, passing the equator in the local morning: MOPITT provides vertically resolved CO observations (individual FOV $\sim 22 \times 22$ km^2, accumulating to over 600 km wide swath FOV) and MODIS supplies information

Table 1. Estimated Average Annual Uncertainty in Determining Fire-Caused Enhancements in CO Concentration Due to Variability in Background CO Levels in the 14 GFED Regions, Defined as in *van der Werf et al.* [2006] (See Also Figure 10)

	Uncertainty Estimate (%)				
Region	**800 hPa**	**700 hPa**	**500 hPa**	**200 hPa**	**Column**
Boreal North America (R1)	20.0	17.5	14.4	58.0	17.7
Temperate North America (R2)	20.5	19.3	14.2	21.7	12.6
Central America (R3)	25.5	20.5	15.8	22.0	14.6
North Hemisphere South America (R4)	20.3	16.5	15.0	20.3	8.4
South Hemisphere South America (R5)	20.4	17.1	18.3	33.0	11.3
Europe (R6)	16.2	13.0	12.8	32.9	10.4
Middle East (R7)	23.5	16.1	12.5	25.7	11.6
North Hemisphere Africa (R8)	33.3	21.3	16.0	20.4	8.9
South Hemisphere Africa (R9)	35.7	32.5	25.0	21.9	18.2
Boreal Asia (R10)	15.3	14.0	12.7	60.4	20.6
Central and East Asia (R11)	18.7	14.2	12.5	34.9	11.8
South and Southeast Asia (R12)	31.0	21.7	15.1	22.4	23.9
Equatorial Asia (R13)	20.1	22.0	23.0	21.3	13.6
Australia (R14)	21.3	20.4	16.2	17.4	14.1

on aerosols and fire counts. The treatment of these data follows the same scheme described above for the A-train sensors. Here we use the MOPITT level 2 V4 CO product, which is currently the latest validated product version. We note that the new MOPITT V5 multispectral product, when adequately validated, promises to have greater sensitivity in the lower troposphere over land [*Worden et al.*, 2010; *Deeter et al.*, 2011].

[9] We assume that the difference between the "fire" CO records, retrieved above simultaneously detected active fire sources, and the long-term monthly mean "background" CO concentrations in a corresponding grid cell can be attributed to biomass burning. This is somewhat akin to aircraft sampled anomalies in fire plumes being evaluated against average background CO concentrations in that region [e.g., *Guyon et al.*, 2005]. This assumption imposes uncertainty on CO estimates, as part of the observed anomalies could be related to other local and nonlocal sources, which will result in an overestimation of the biomass burning contribution. Likewise, if the true background CO concentration at the time of measurement was lower than average, this method will lead to an underestimate of fire-emitted CO. The associated uncertainty can be characterized by analyzing the variation of "background" CO around the average concentrations. At the lower pressure levels, this results in ~20% uncertainty on a global scale, with highest uncertainty (30–35%) in Africa and South and Southeastern Asia (Table 1), which exhibit the highest variability in "clear" background CO concentrations. The largest uncertainties (~60%) are found at the 200 hPa pressure level in the Boreal regions. Emissions per fire count (EPFC) rates are obtained by dividing the total column difference between "fire" and "background" CO by the corresponding MODIS fire counts recorded at this grid cell.

3. Climate Model

[10] We use simulations performed with the newer version of Model-E [*Schmidt et al.*, 2006], the model of atmospheric composition and climate developed at the NASA Goddard Institute for Space Studies (GISS). The new version, called Model-E2, is similar to the previous model but has numerous improvements to the physics, including the ability to represent multiple downdrafts and updrafts in convective systems. This improved representation of vertical airflow enhances the model's ability to represent vertical transport of biomass burning CO emissions and is especially important in the tropics. Detailed description of composition simulated in GISS Model-E2 as well as evaluations against available observations can be found in *Shindell et al.* [2013]. Model runs analyzed here were performed at $2° \times 2.5°$ horizontal resolution, with 40 vertical layers extending to 0.1 hPa. Biomass burning emissions were prescribed on a monthly basis from GFED2 and GFED3 emission databases.

4. CO Profile Retrieval

[11] TES uses Fourier transform spectroscopy to convert measured infrared (IR) radiance from the Earth's surface and atmospheric constituents into emission spectra. MOPITT measures IR radiances in CO and methane absorption bands using gas-filter correlation radiometry. The emission/absorption wavelengths depend on atmospheric concentrations and vary with temperature and pressure, which are altitude dependent. Hence, with precisely measured spectra, the altitude of chemical species can be retrieved using the optimal estimation method [*Rodgers*, 2000]. This method, followed in both the TES [*Bowman et al.*, 2002; *Worden et al.*, 2004] and MOPITT [*Deeter et al.*, 2003] retrieval processes, requires a priori assumptions for the atmospheric profiles to constrain retrieval results and obtain a unique solution. The retrieved profile x_{ret} may be expressed as a linear combination of the (unknown) true atmospheric profile x weighted by the averaging kernel matrix A, the a priori profile x_a, and the retrieval error ε (equation (1)).

$$x_{ret} = Ax + (I - A)x_a + \varepsilon \tag{1}$$

[12] The averaging kernels are determined by sensitivities of spectral measurements to species concentrations at different pressure levels, signal-to-noise ratios, and retrieval a priori constraints. In the ideal case of $A = I$ (unity matrix), the retrieved profile would equal the true profile x plus noise ε. However, the averaging kernels of both TES and MOPITT are far from unity, and hence, the a priori assumptions x_a have nonnegligible influence on x_{ret}, dominating low-sensitivity retrievals.

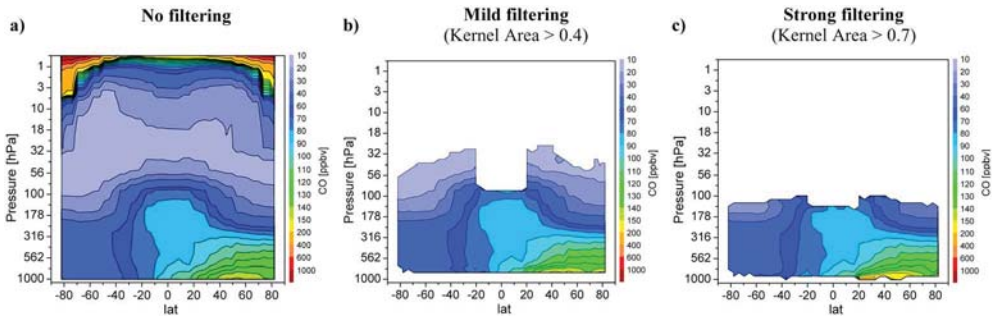

Figure 2. TES 2005–2008 annual mean zonally averaged CO retrievals (a) without filtering low-sensitivity data and (b) with mild and (c) strong filtering applied.

5. Sensitivity Filtering

[13] To avoid a situation where a significant volume of analyzed data reflects a priori assumptions rather than actual measurements, we filter retrievals that are dominated by the a priori. A common filtering parameter is the diagonal term of the averaging kernel matrix [*Zhang et al.*, 2008], which indicates how sensitive the retrieval at a specific pressure level was to the true atmospheric state at that pressure level. However, even if the retrieval at the level of interest has a low diagonal term value, measurements at other pressure levels might have been sufficient to retrieve meaningful concentrations at the level of interest. This can be accounted for by instead using the averaging kernel area (*ka*) as a filtering parameter [*Lopez et al.*, 2008]. The *ka* is a measure of the information obtained from measurements at all levels when solving for a retrieval at a certain level. Here we adopt this latter method, and since TES sensitivities are generally lower than those of MOPITT [*Luo et al.*, 2007], we will more closely examine TES data to establish our filtering conditions.

[14] Figure 2a shows TES 2005–2008 annual mean zonally averaged CO retrievals with no sensitivity filtering applied. Figure 2b shows the same data after "mild filtering" requiring $ka \geq 0.4$, which corresponds approximately to demanding that at least 40% of retrieval information come from measured data rather than a priori. This has filtered out virtually all data above ~30 hPa and much of the near-surface retrievals, which were largely reflecting a priori assumptions rather that actually measured atmospheric conditions. Applying yet stronger filtering of $ka \geq 0.7$ (Figure 2c) removes virtually all data above ~100 hPa, leaving only the more reliable retrievals in the troposphere. Note that other than "wiping out" levels of less reliable data, filtering causes little change in the atmospheric concentrations at most of the remaining pressure levels, as TES average sensitivities are generally systematically higher at these altitudes (Figure 3).

[15] At the lower levels, however, the differences are prominent. This is clearly seen in the plots of Figure 4 showing 2005–2008 annual mean TES CO retrievals at about 800 hPa with "mild" and "strong" filtering compared to CO simulated with GISS Model-E2 smoothed with TES averaging kernels and relaxed toward TES a priori (equation (1)). Such processing of modeled CO mimics the TES retrieval procedure, showing what TES would have retrieved if the true atmosphere was identical to the modeled one. When mild filtering is applied to the data, the model and TES show very good agreement in the spatial distribution of CO concentrations (Figure 4a). However, when stronger filtering is applied (Figure 4b), the two become notably different, and the agreement between TES and the model is preserved only where retrievals on average have higher sensitivity (Figure 5a). The reason for such large differences when comparing TES and modeled retrievals of different sensitivities is twofold. When comparing TES and the TES-processed model, we basically compare TES measured content plus some TES a priori content with modeled content plus the same TES a priori. By mildly filtering data, we allow a considerable amount of a priori content in the comparisons, which is the same for both TES and modeled data and inevitably yields better correlations between the two. Note, for instance, how TES-retrieved and modeled CO concentrations in North America, which are very different in the higher sensitivity retrievals (Figure 4b), become very similar in the lower sensitivity retrievals (Figure 4a), which are more influenced by the a priori assumptions (Figure 5b). On the other hand, when applying stronger filtering, we end up with too little "good" data in areas where sensitivities are generally lower, and comparisons may become unreliable. These aspects should be kept in mind when analyzing satellite-retrieved information, and in particular, they imply much greater reliability in the tropics (Figure 5a). In our further analysis, we apply "strong" filtering to all data to minimize the influence of a priori assumptions.

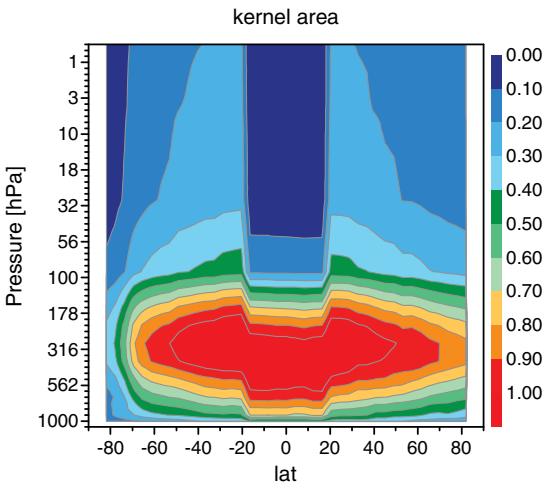

Figure 3. TES 2005–2008 annual mean zonally averaged kernel area (*ka*) of CO retrievals.

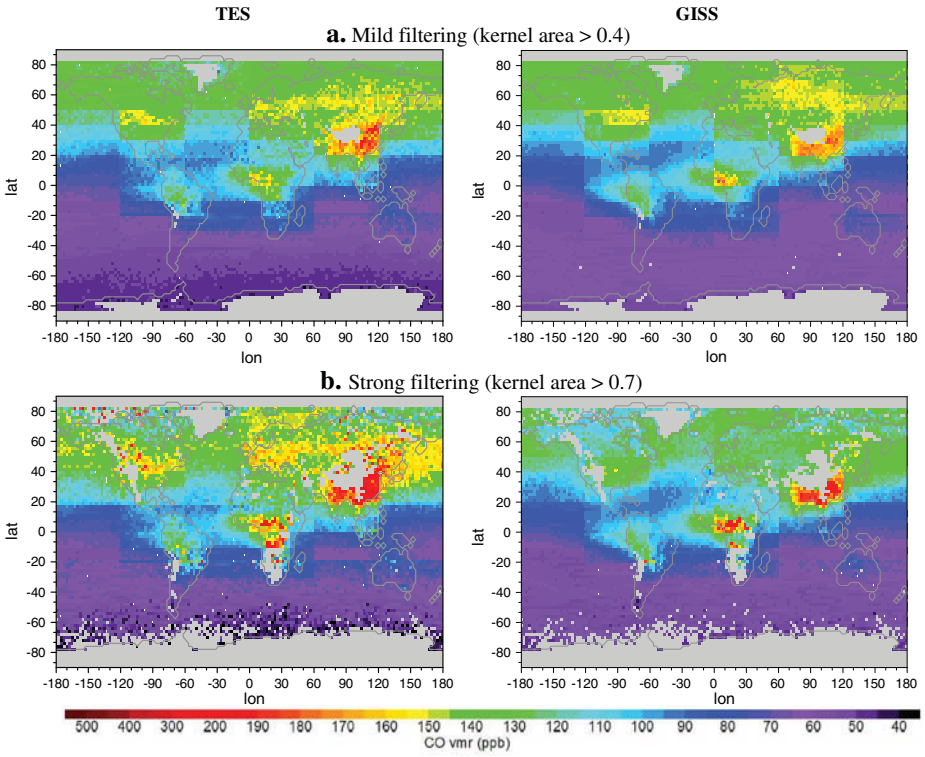

Figure 4. 2005–2008 annual mean TES CO retrievals at about 800 hPa with (a) mild and (b) strong filtering compared to CO simulated with GISS Model-E2 and processed with TES averaging kernels and a priori.

6. "Fire" Versus "Background" CO: Observations and Modeling

[16] Separated "fire" and "background" TES CO records (Figure 6a) show concentrations associated with tropical afternoon fire activity that are much larger than the "background" values at the lower pressure levels (800 and 700 hPa). Modeled CO simulated with GFED prescribed fire emissions was sampled with each satellite's overpass times and locations, using corresponding averaging kernels and a priori assumptions (equation (1)). These TES-processed modeled tropical concentrations are significantly lower than "fire" CO concentrations retrieved by TES at 800 and 700 hPa (Figure 6a). "Background" concentrations, however, are relatively well depicted. With height, both "fire" and "background" modeled CO concentrations become high-biased comparing to TES. This supports the suggestion raised in a different study [*Shindell et al.*, 2013] that increasing TES model biases with height likely result from too large a ratio of CO production from hydrocarbon oxidation relative to CO's own oxidation rather than being related to convection within the model transporting CO too rapidly from surface sources to the upper troposphere.

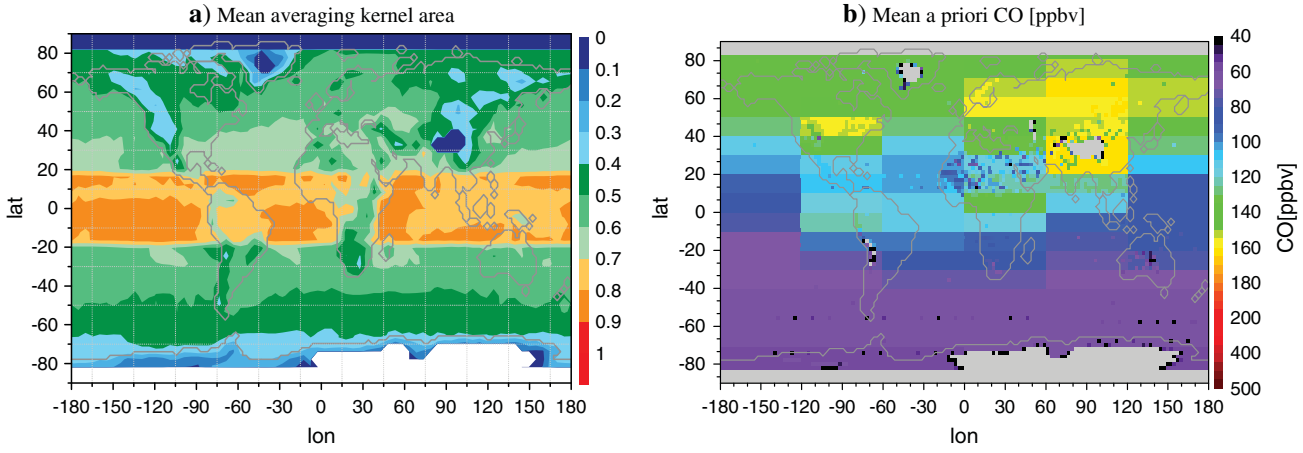

Figure 5. (a) 2005–2008 annual mean averaging kernel area (*ka*) and (b) mean a priori for TES CO retrievals at about 800 hPa.

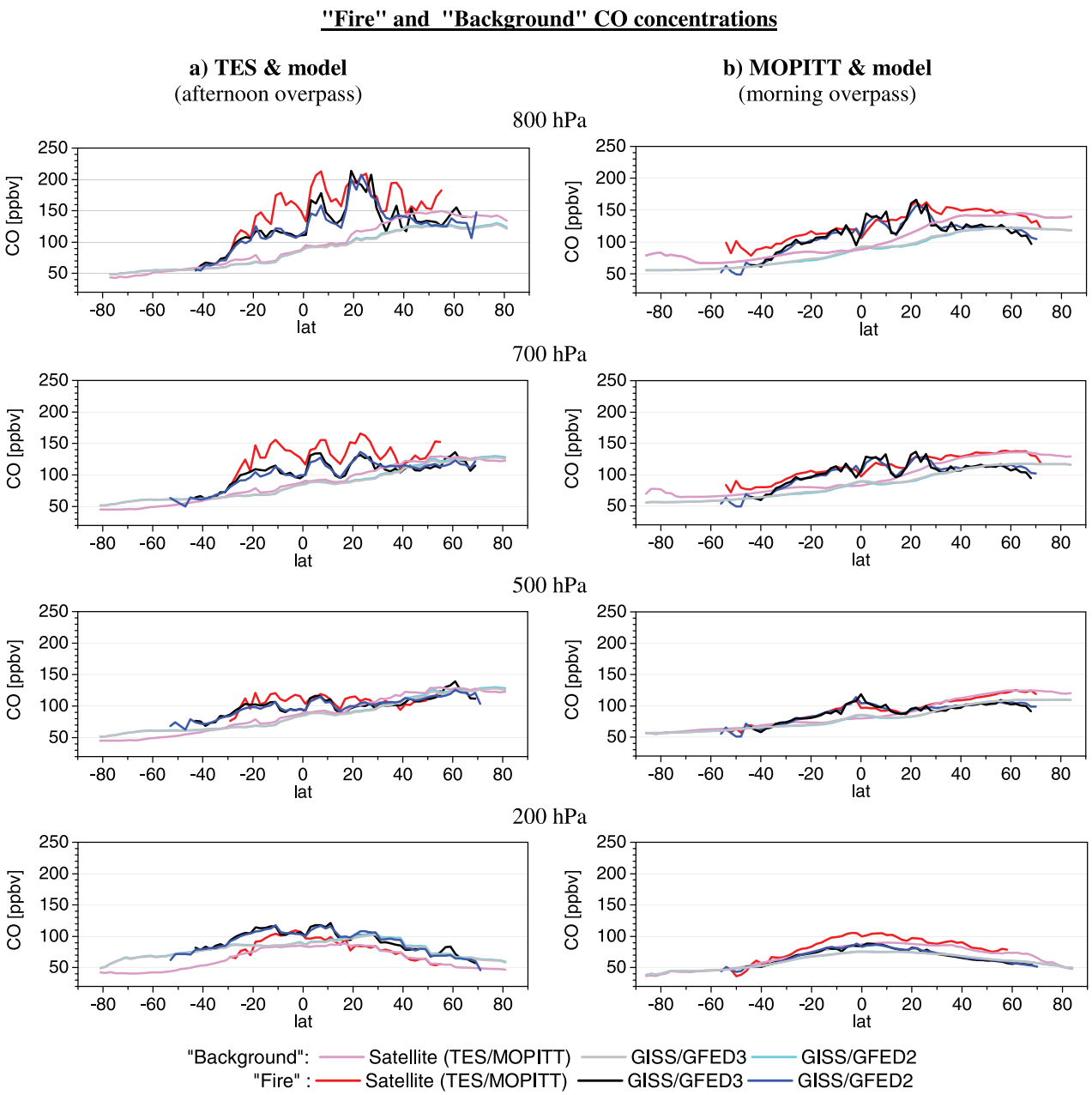

Figure 6. 2005–2008 annual mean zonally averaged "Fire" and "Background" CO retrieved with TES and MOPITT and simulated with GISS Model-E2 using GFED v.2.1 and GFED3 fire emissions.

[17] Tropical "fire" CO concentrations observed with MOPITT are much lower than TES at 800 hPa (Figure 6b). This is despite TES CO retrievals being generally biased low compared to MOPITT [*Ho et al.*, 2009]. To facilitate comparison between TES and MOPITT results, these MOPITT retrievals were adjusted to TES a priori [*Luo et al.*, 2007]. Hence, the differences between TES and MOPITT "fire" CO records presented here do not result from different a priori assumptions. (This adjustment, however, did not have a large influence on our results since filtered data are less influenced by a priori assumptions.) One of the probable reasons for different TES and MOPITT tropical "fire" CO concentrations is their overpass time. MOPITT passes the equator in the local morning while TES flies within the afternoon constellation, recording the tropical fire activity at its strongest [*Giglio*, 2006].

[18] MOPITT-processed model concentrations are generally close to MOPITT observations (Figure 6b), although MOPITT concentrations are notably higher in the northern extratropics. It is generally accepted that high latitude MOPITT CO retrievals should be used with caution [*Arellano et al.*, 2004]. At mid latitudes, low-biased CO is found in many models [*Shindell et al.*, 2006]. Seasonal underestimate in biomass burning emissions in the inventories was suggested as the most probable candidate for these biases [*Shindell et al.*, 2006; *Kopacz et al.*, 2009]. Note,

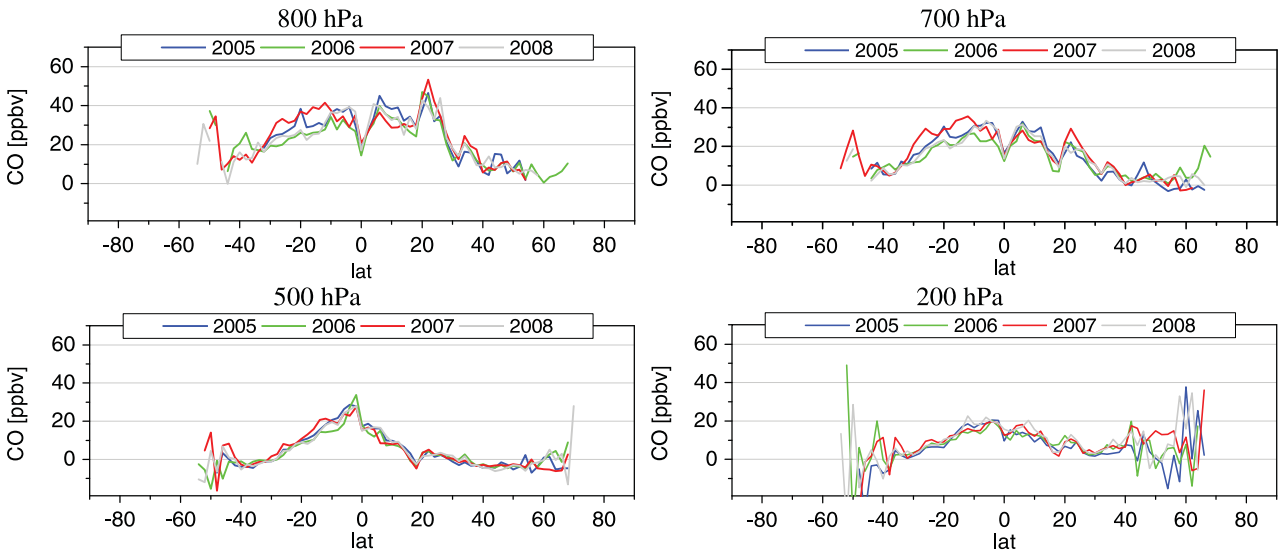

Figure 7. Annual mean zonally averaged "Fire"-"Background" CO concentration differences retrieved with MOPITT for years 2005–2008.

however, that modeled "background" concentrations are low-biased at these latitudes, comparing to both MOPITT and TES, suggesting that there are additional reasons for the observed disagreements. The "fire"-"background" CO concentration differences retrieved with MOPITT are quite robust across the years in the lower and middle troposphere. In the upper troposphere, however, results are robust equatorward of about 40°, where convective activity more effectively communicates surface concentrations to the troposphere, while variability is very large at high latitudes (Figure 7 and Table 1).

[19] To further characterize the ability of our methodology to capture the true impact of fires on CO, we compared analysis of the model's CO based on the "fire"-"background" segregation method with the total influence of biomass burning CO in the model determined by running a separate simulation with biomass burning emissions turned off. The modeled "background" concentrations are on average 7–15% higher than concentrations in the simulation without biomass burning, due to fire emissions diluted from distant sources. This leads to a low bias of ~9–24% in regions with sizable CO from fires (at least 10% above background) using our "fire" minus "background" methodology. This characterizes the low bias such dilution may impose on segregated fire CO concentrations and indicates that the biomass burning emission estimates reported here are likely slightly conservative.

7. Emissions per Fire Count Factors: TES, MOPITT and GFED Inventory

[20] Exploiting the advantage of near-simultaneous MODIS active fire records, we can look at TES and MOPITT CO emissions rates per MODIS fire count (EPFC). Examining EPFCs rather than emissions diminishes the influence of diurnal fire activity variations in comparisons. We compare TES and MOPITT EPFCs directly to EPFCs in GFED inventories [*van der Werf et al.*, 2006], which are also based on MODIS active fires; hence, there is no atmospheric modeling in the following analysis.

[21] Since MOPITT observes CO up to 100 hPa, TES column values used to compute EPFCs were also taken up to 100 hPa. However, calculating TES EPFCs from total column yields virtually indistinguishable results, since "fire" CO concentrations drop quite rapidly with height (Figure 6) and have little contribution at high pressure levels.

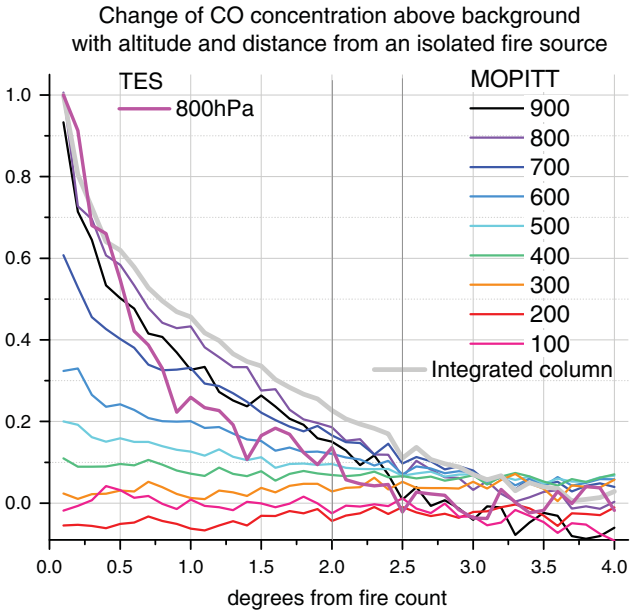

Figure 8. Change of fire-related enhancement of MOPITT CO concentrations above background with altitude and distance from the fire source, normalized by the enhancement above source at 900 hPa; integrated MOPITT column normalized by the above-source value; and TES CO enhancement at 800 hPa, also normalized by the above-source value.

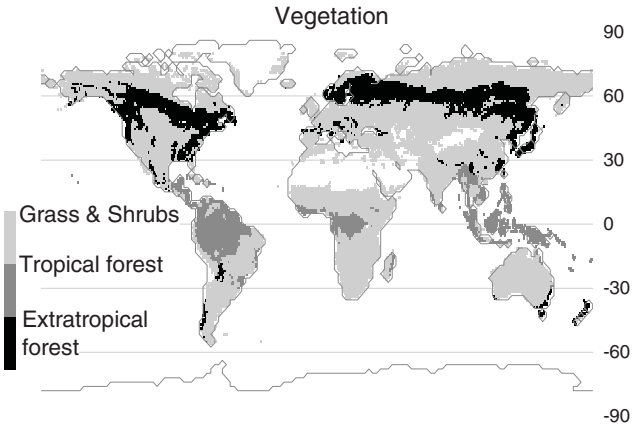

Figure 9. Three basic vegetation types used in the GFED database [*van der Werf et al*., 2006].

[22] We calculate EPFCs as a difference between fire-related and background CO integrated over the vertical column and divided by the number of MODIS fire counts at that grid cell. This procedure imposes low bias on the estimates, as not all emitted CO is located within the grid cell due to horizontal transport. Analysis of MOPITT CO concentrations retrieved for nearly a hundred isolated MODIS fire events in the year 2007 shows that at the lower levels, CO enhancement above the background decreases rapidly with distance from the fire source (Figure 8). TES retrievals at 800 hPa for the same year show quite similar behavior (Figure 8). (Due to its very small FOV, retrieving TES CO at increasing distances from a specific fire is impossible; hence, instead, we determined distance to closest active fire for each CO retrieval.) MOPITT retrievals show CO enhancement above fires decreasing with altitude, and above 500 hPa, it is already not much different from the remote values. As the fire-induced enhancement decreases, its separation from background becomes less certain. Hence, this analysis cannot strongly constrain the dilution of emissions into the neighboring cells at the upper levels but helps quantify the amount of potential transport after emission in the lower troposphere, where the impact from fire activity is strongest. These lower troposphere levels contribute most to the enhancement of integrated column CO, which outside the gridbox ($2° \times 2.5°$) reduces to values too low to allow reliable separation of the near-fire areas from the background, quickly falling well within the uncertainty limits (Table 1). Hence, sampling directly over the gridbox, we account for the major and the most reliably determined portion of CO enhancement over fires, although missing some dilution (about 20%) due to horizontal transport, which gives a systematic low bias in the following calculations.

[23] To facilitate easier comparison, we grouped the obtained EPFCs into three basic vegetation types (Figure 9) dominating each grid cell in the 14 regions (Figure 10) that were used in deriving the GFED database [*van der Werf et al*., 2006]. The annual-mean EPFCs averaged over these vegetation types and regions are shown in Figure 11. Estimated uncertainty in determining fire-related enhancements in CO concentration for these regions is given in Table 1 (typically 10–30%). In many regions, TES has too few records to provide any reliable estimates. In further discussion, we will largely disregard estimates derived based on fewer than 100 records. In Figure 11, bars showing such estimates are shaded out with a white diagonal pattern (the number of available TES records appears on the bars). The deviations of GFED EPFCs from MOPITT values for each region and vegetation type are shown in Figure 12, along with an indication of statistical significance for the GFED3 versus MOPITT differences with respect to uncertainties in this method (due to background variability and horizontal transport) and uncertainties in GFED3 estimates [*van der Werf et al*., 2010].

[24] In many regions, GFED3 emission rate estimates from extratropical forests agree much better with MOPITT than the older GFED2 database (Figures 11 and 12). Europe (R6) and Southern Hemisphere (S. Hem.) South America (R5) are the most notable examples. Tropical forests emission rates are also much closer to MOPITT in the GFED3 database, whereas in GFED2, they were generally overestimated. In most regions, adjusting MOPITT records to TES a priori has a minute effect (Figure 11); however, in Southeastern and Equatorial Asia (R12 and R13), this process reduces the values and brings them considerably closer to GFED levels. Using only higher-sensitivity records diminishes but does not completely remove a priori influence, and it is unclear whether TES or MOPITT a priori assumptions (both are temporally and spatially variable) yield more realistic estimates here. In the tropical forests of S. Hem. South America (R5), one of the few regions where TES records are relatively abundant, all data sets agree well (Figure 11). Although differences in emission rate estimates for tropical forests are often large between the two GFED databases, they have little effect on the actual CO emissions, as this vegetation is less fire prone.

[25] In most regions, the grass/shrubs vegetation class shows relatively little difference between the two GFED databases, and both are generally underestimated compared to MOPITT (Figures 11 and 12). In some regions, the older GFED2 estimates for grass/shrubs emission rates are closer to MOPITT (e.g., tundra (R1 and R10) and Europe (R6)), while in others, the newer GFED3 estimates agree better with the satellite (e.g., Equatorial Asia (R13)). Although differences between GFED3 and MOPITT are quite large in the Northern Hemisphere high latitudes (boreal regions R1 and

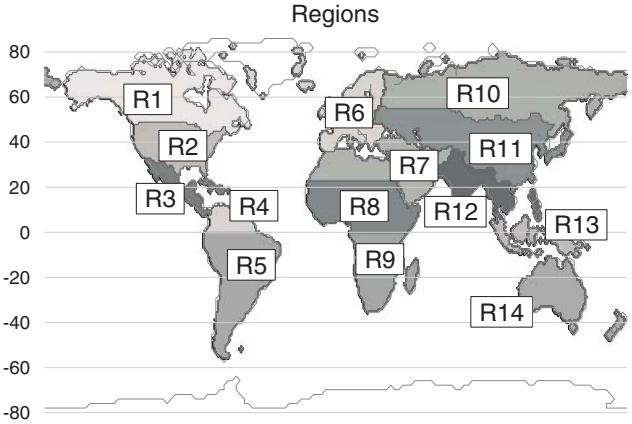

Figure 10. The 14 regions used in the GFED database [*van der Werf et al*., 2006].

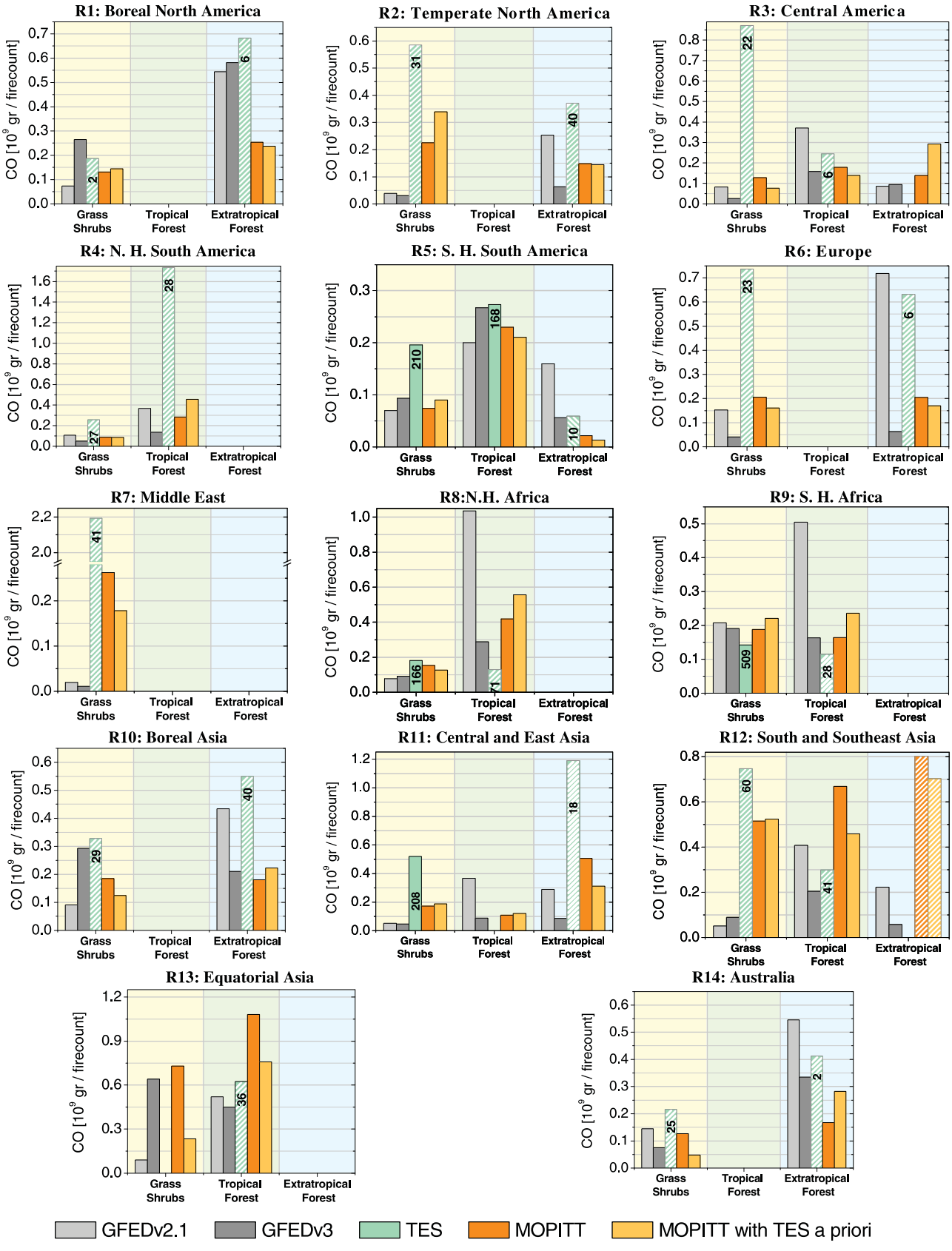

Figure 11. 2005–2008 annual mean CO emissions per MODIS fire count derived from TES and MOPITT and from GFED2 and GFED3 databases for the 14 GFED regions (Figure 10) and the three basic vegetation types (Figure 9). Numbers on the TES bars indicate the number of retrievals this record comprises. The bars are shaded out with white diagonal pattern whenever the number of records is less than 100.

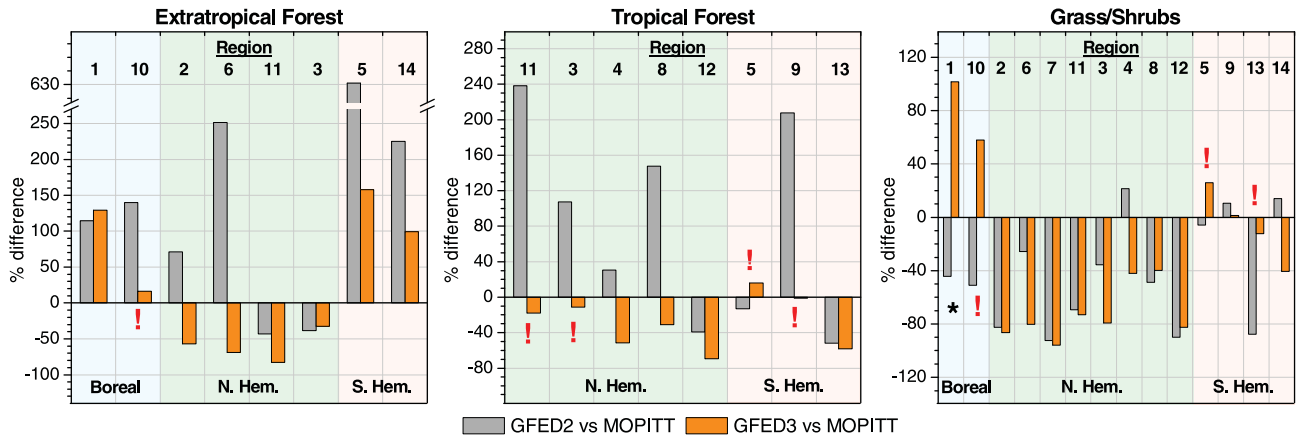

Figure 12. GFED2 and GFED3 versus MOPITT 2005–2008 annual mean CO emissions per MODIS fire count for the 14 GFED regions and the three basic vegetation types. GFED3 vs MOPITT differences are statistically significant within 5% (p=0.05), except for those indicated with (*) = low significance (10%) and (!) = statistically insignificant.

R10), they are statistically insignificant given the large uncertainties in GFED3 [*van der Werf et al.*, 2010] and this method for those regions (Figure 12). In African grass and shrubs (R8 and, especially, R9), where fire activity is highest and TES information is quite plentiful, EPFCs in all data sets correspond reasonably (Figure 11). MOPITT emission rates in South and Southeast Asia (R12) are significantly higher than in both GFED databases, fortifying the growing evidence that CO emissions in Asia are significantly underestimated in current inventories [*Petron et al.*, 2002; *Arellano et al.*, 2004]. Biomass burning black carbon (BC) emissions were also found to be greatly underestimated in South Asia [*Bond et al.*, 2013]. In the Middle East (R7), the differences between GFED and MOPITT and between MOPITT and TES are an order of magnitude (Figure 11). Disagreement between GFED and satellites may result from potentially inappropriate identification of vegetation type. While grass and shrubs dominate this region, they may not be the dominant burning vegetation type, as they are largely croplands and rarely burn due to close human control. Thus, emission factors derived from satellite observations here may actually relate to different vegetation type. The number of available fire-related TES observations in this region is too low to provide a trustworthy emission rate estimate, but the order-of-magnitude difference with MOPITT warrants a closer examination.

[26] Figure 13a shows the occurrence frequency of different EPFC values in the grass/shrubs vegetation type in the Middle East for MOPITT and TES. It turns out that values derived from TES do not exceed the range of MOPITT retrievals. However, while the occurrence frequency of larger values is comparable for both sensors, the lower values are much more frequently encountered with MOPITT. Such a large range of emission rates observed by the same sensor in the same region most probably arises from recording fires occurring in different ambient conditions, e.g., fuel moisture, horizontal winds changing emissions dispersion, vegetation density, and/or different vegetation types (GFED vegetation type is the dominant one, but not the sole type in the region). It would be reasonable to assume that, in general, lower emission amounts are produced by weaker, smaller, shorter-lived fires. Such fires are much more likely to be missed by TES with its very small FOV than the larger and more persistent fires. MOPITT has a much larger FOV and hence a much higher chance to encounter smaller fires. It therefore appears that

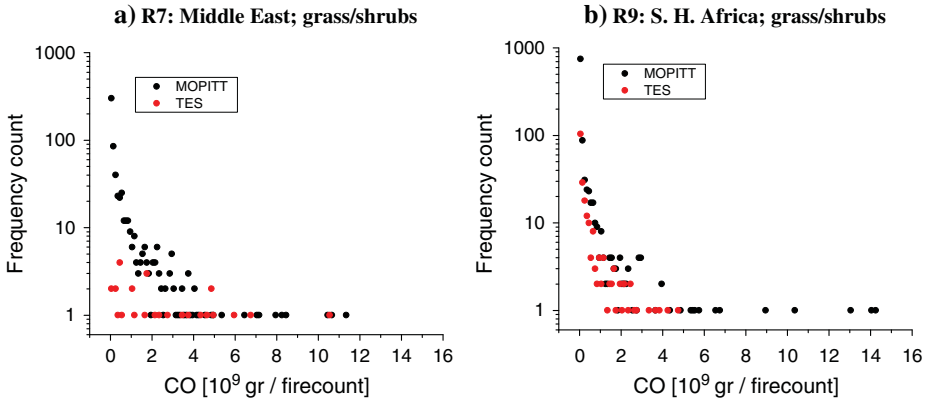

Figure 13. Occurrence frequency of different emission rates for MOPITT and TES for (a) Middle East grass/shrubs (23 TES "fire" records) and (b) South Hemisphere Africa grass/shrubs (608 TES "fire" records).

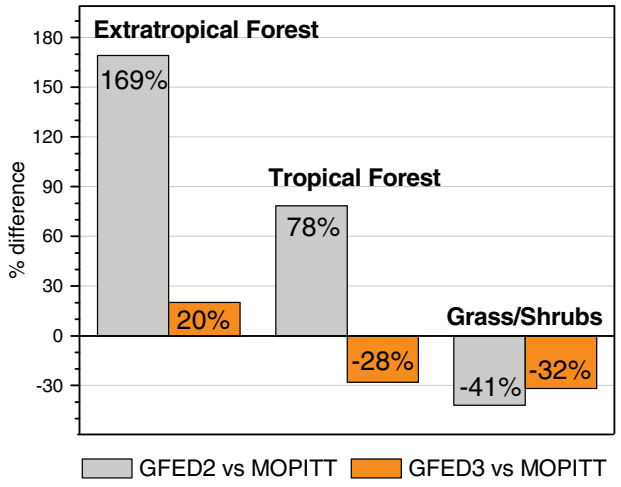

Figure 14. Global mean difference (in percent) between the two GFED inventories and MOPITT 2005–2008 annual mean CO emissions per MODIS fire count rates for the three basic vegetation types.

while the range of observed values is similar for both sensors, TES tends to see the larger fires, so TES emission estimates tend to be higher, especially when the number of available retrievals is low. This may be an additional factor accounting for the generally higher emissions observed with TES compared to MOPITT (Figure 6). As the number of TES records increases, e.g., in a tropical area such as Southern Hemisphere Africa, so do its chances to encounter a wider variety of events, and occurrence frequencies approach those of MOPITT (Figure 13b). Inevitably, the large differences in FOV and capacity to observe fires of different sizes make comparison between TES and MOPITT (Figures 6 and 11) difficult where TES data are scarce (specifically outside the tropical region).

[27] On average, emission rates in the newer GFED3 inventory show a far better correspondence to MOPITT than the older database (Figure 14). However, for grasses and shrubs, the most globally prevailing and most fire-prone vegetation type, there was little change, and the GFED emission rates remain underestimated compared to MOPITT.

8. Seasonal CO Variations

[28] MOPITT provides a sufficiently large number of fire-related CO records to infer meaningful monthly variations in the four major latitude belts, and we compare them to data modeled with prescribed GFED3 and GFED2 fire emissions (Figure 15).

[29] Overall, MOPITT and modeled seasonal variations agree quite reasonably. In the northern extratropics (Figure 15a), the model underestimates CO concentrations compared to MOPITT throughout the whole year. MOPITT tends to be 5–11% high-biased, especially in the Northern Hemisphere [*Emmons et al.*, 2004, 2007, 2009; *Jacob et al.*, 2003], which can account a portion for these year-round differences. However, there is also a seasonal component (Figure 15a). Increased spring biases in the "fire" CO concentrations strengthen the suggestions that emission inventories have considerable seasonal underestimates in the northern extratropics, causing systematical seasonal underestimate of CO concentrations in composition and climate models [*Shindell et al.*, 2006; *Kopacz et al.*, 2010]. However, seasonal winter-spring increase in the "background" biases provides supporting evidence for the hypothesis that modeling biases in northern extratropics should not be attributed solely to biomass burning inventories and may result from other unaccounted sources, like vehicle cold starts and residential heating [*Kopacz et al.*, 2010].

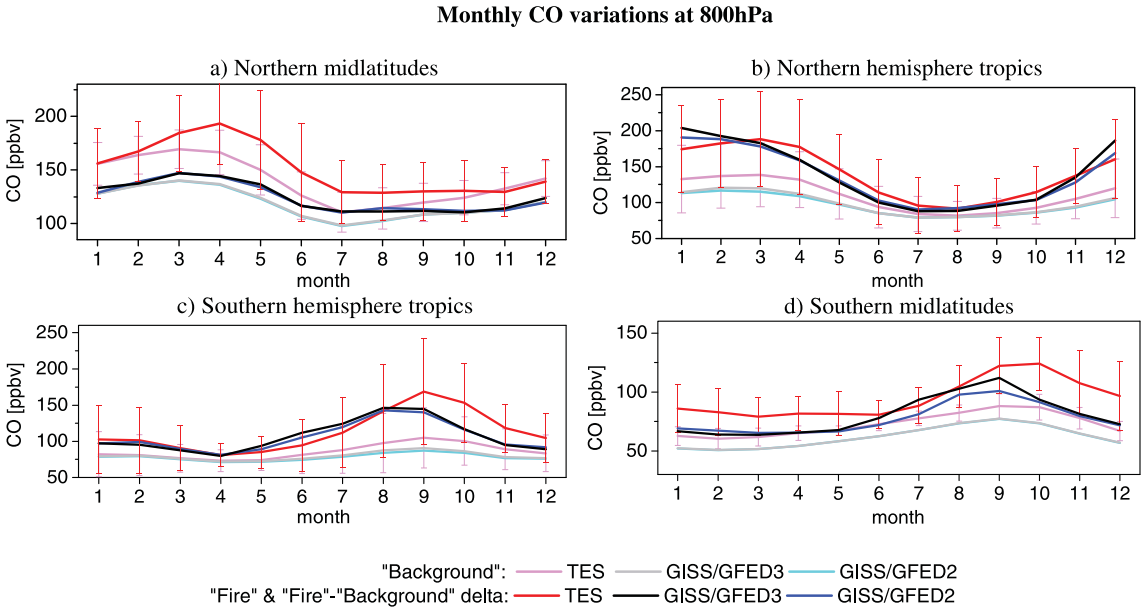

Figure 15. 2005–2008 seasonal variations of CO concentrations retrieved from MOPITT and modeled with GISS Model-E2 with GFED2 and GFED3 prescribed biomass burning emissions in (a) northern midlatitudes (30 N–60 N), (b) Northern Hemisphere tropics (0–30 N), (c) Southern Hemisphere tropics (0–30° S), and (d) southern midlatitudes (30°S–60°S).

[30] In the tropics (Figures 15b and 15c), MOPITT and modeled CO concentrations agree well. In the Southern Hemisphere tropics, however, the model using GFED produces a fire season shifted approximately one month early (Figure 15c). This agrees with seasonality mismatch found between GFED and other top-down (inverse) CO estimates in Southern Hemisphere Africa [*van der Werf et al*., 2006]. In the southern extratropics, the GFED-based model shows the same shift in the fire season compared to MOPITT (Figure 15d). This is while "background" seasonal variations are well depicted, though somewhat low-biased, providing a strong indication that the biomass burning emissions are underestimated. The differences between the two GFED databases are most apparent here, with the GFED3 inventory providing closer correspondence to MOPITT.

9. Discussion

[31] Analysis of emission rates derived from fire-related satellite CO retrievals and fire counts against GFED bottom-up emission rate estimates shows that, on the regional scale, there are often substantial difference between GFED3-, GFED2-, and MOPITT-based emission rates. In general, GFED3 shows a far better agreement with MOPITT in tropical and extratropical forests but only slightly better agreement in grasses and shrubs. GFED3 extratropical forest emission rates are ~20% overestimated compared to MOPITT-based estimates, although this may in part reflect the low bias in our methodology. Emissions from tropical forests and grass/shrubs are generally ~30% underestimated despite MOPITT-based values being systematically biased low due to both sampling directly over fire gridbox and missing some dilution (~20%) due to horizontal transport and the weak impact of diluted remote emissions on the background. In South and Southeast Asia, MOPITT-based emission rates are significantly higher than in both GFED databases, despite their low bias, strengthening evidence that current inventories underestimate Asian CO emissions. A drastic, order-of-magnitude difference is found between GFED- and MOPITT-based emission rates in the Middle East, possibly due to improper identification of the main burning vegetation type: a large portion of the grass/shrubs dominating this region are croplands that rarely burn; hence, satellite-derived emissions may actually relate to a different vegetation type.

[32] "Fire" CO concentrations modeled with both inventories and retrieved from MOPITT agree reasonably well on global scales, although substantial underestimates (30%) in the models are found in the Northern Hemisphere spring. This suggests an underestimate of biomass burning CO emissions in the Northern Hemisphere spring, which would partially account for the seasonal low biases seen in many models at these latitudes. However, there are also seasonal underestimates in the "background" CO concentrations, indicating that these biases may have additional sources (i.e., residential heating). In the Southern Hemisphere, the model using GFED produces a fire season one month shorter than that observed by MOPITT, while "background" seasonality is well depicted, providing a strong indication that Southern Hemisphere September-October-November biomass burning emissions are underestimated in the GFED inventory.

[33] TES retrievals indicate tropical fire CO emissions about twice as high as either GFED or MOPITT. It appears that due to its small FOV and scarcity of fire-related retrievals, TES records predominantly larger fires. Moreover, TES passes over the tropics in the afternoon, when fire activity is strongest, while MOPITT has a morning overpass time. Outside the tropical region, where the number of available fire-related TES retrievals is generally low, differences in FOV and capacity to observe fires from different sizes make the comparison between TES and MOPITT uncertain. Similar to earlier studies, model runs analyzed here prescribed the GFED inventory on a monthly basis and hence do not depict the magnitude of the afternoon peak.

[34] Emission estimates obtained with inversion top-down methods are significantly influenced by modeling biases, often producing substantially different results depending on the model used [e.g., *Jiang et al*., 2011, 2013]. Those top-down estimates tend to differ considerably from bottom-up inventories, some showing as much as 60% disagreement in biomass burning CO emissions [*Kopacz et al*., 2010]. This study is a step toward bringing the two methods closer to a common ground. Separating CO observations over active fire sources from the background allowed us to more directly study satellite-retrieved biomass burning emissions without invoking inverse modeling as in traditional top-down approaches. Attributing CO anomalies at active fire locations explicitly to biomass burning is estimated to introduce on average ~20–30% uncertainty. However, this method may be unsuitable for case studies, as for each and every measurement, the associated error may be considerably larger due to higher than average influence of other CO sources (i.e., upwind anthropogenic sources). Moreover, at high latitudes, where CO concentrations are less effectively transferred from the source to the troposphere, uncertainties increase significantly aloft. Although we still find considerable regional differences between satellite-retrieved and bottom-up biomass burning emission estimates, on global scales, they appear to be in better agreement than previously thought. Specifically, the newer GFED3 inventory is found to be globally in quite reasonable agreement with MOPITT estimates (with average differences of ~30%). Despite the huge volumes of data provided by the satellites, just a fraction proved to satisfy high-sensitivity requirements, and in many regions, the number of retrievals associated with fire activity was very low. Thus, it was not always possible to meaningfully compare between TES and MOPITT retrievals or perform more spatially and temporary resolved analysis. There is a need for further research incorporating additional satellite sensors and model simulations with subdaily prescribed emissions, and there is also a need for improved satellite CO data.

References

Andreae, M. O., and P. Merlet (2001), Emission of trace gases and aerosols from biomass burning, *Global Biogeochem. Cycles*, *15*, 955–966.

Arellano, A. F., Jr., and P. G. Hess, (2006), Sensitivity of top-down estimates of CO sources to GCTM transport, *Geophys. Res. Lett.*, *33*, L21807, doi:10.1029/2006GL027371.

Arellano, A. F., Jr., P. S. Kasibhatla, L. Giglio, G. R. van der Werf, and J. T. Randerson (2004), Top-down estimates of global CO sources using MOPITT measurements, *Geophys. Res. Lett.*, *31*, L01104, doi:10.1029/2003GL018609.

Bian, H., M. Chin, S. R. Kawa, B. Duncan, A. Arellano, and P. Kasibhatla (2007), Sensitivity of global CO simulations to uncertainties in biomass burning sources, *J. Geophys. Res.*, *112*, D23308, doi:10.1029/2006JD008376.

Bond T. C., et al. (2013), Bounding the role of black carbon in the climate system: A scientific assessment, *J. Geophys. Res. Atmos.*, *118*, 5380–5552, doi:10.1002/jgrd.50171.

Bowman, K. W., J. Worden, T. Steck, H. M. Worden, S. Clough, and C. Rodgers (2002) Capturing time and vertical variability of tropospheric ozone: A study using TES nadir retrievals, *J. Geophys. Res.*, *107*(D23), 4723, doi:10.1029/2002JD002150.

Deeter, M. N., et al. (2003), Operational carbon monoxide retrieval algorithm and selected results for the MOPITT instrument, *J. Geophys. Res.*, *108*(D14), 4399, doi:10.1029/2002JD003186.

Deeter, M. N., H. M. Worden, J. C. Gille, D. P. Edwards, D. Mao, and J. R. Drummond (2011), MOPITT multispectral CO retrievals: Origins and effects of geophysical radiance errors, *J. Geophys. Res.*, *116*, D15303, doi:10.1029/2011JD015703.

Emmons, L. K., et al. (2004), Validation of Measurements of Pollution in the Troposphere (MOPITT) CO retrievals with aircraft in situ profiles, *J. Geophys. Res.*, *109*, D03309, doi:10.1029/2003JD004101.

Emmons, L. K., G. G. Pfister, D. P. Edwards, J. C. Gille, G. Sachse, D. Blake, S. Wofsy, C. Gerbig, D. Matross, and P. Nedelec (2007), Measurements of Pollution in the Troposphere (MOPITT) validation exercises during summer 2004 field campaigns over North America, *J. Geophys. Res.*, *112*, D12S02, doi:10.1029/2006JD007833.

Emmons, L. K., D. P. Edwards, M. N. Deeter, J. C. Gille, T. Campos, P. Nédélec, P. Novelli, and G. Sachse (2009), Measurements of Pollution In The Troposphere (MOPITT) validation through 2006, *Atmos. Chem. Phys.*, *9*, 1,795–1,803.

Giglio, L. (2006), Characterization of the tropical diurnal fire cycle using VIRS and MODIS observations, *Remote Sens. Environ.*, *108*, 407–421.

Giglio, L., G. R. van der Werf, J. T. Randerson, G. J. Collatz, and P. S. Kasibhatla (2006), Global estimation of burned area using MODIS active fire observations, *Atmos. Chem. Phys.*, *6*, 957–974. SRef-ID: 1680-7324/acp/2006-6-957.

Giglio, L., T. Loboda, D. P. Roy, B. Quayle, and C. O. Justice (2009), An active-fire based burned area mapping algorithm for the MODIS sensor, *Remote Sens. Environ.*, *113*, 408–420, doi:10.1016/j.rse. 2008.10.006.

Giglio, L., J. T. Randerson, G. R. van der Werf, P. S. Kasibhatla, G. J. Collatz, D. C. Morton, and R. S. DeFries (2010), Assessing variability and long-term trends in burned area by merging multiple satellite fire products, *Biogeosciences*, *7*, 1,171–1,186, doi:10.5194/bg-7-1171-2010.

Gonzi, S., P. I. Palmer, M. P. Barkley, I. De Smedt, and M. Van Roozendael (2011), Biomass burning emission estimates inferred from satellite column measurements of HCHO: Sensitivity to co-emitted aerosol and injection height, *Geophys. Res. Lett.*, *38*, L14807, doi:10.1029/2011GL047890.

Guyon, P. et al. (2005), Airborne measurements of trace gas and aerosol particle emissions from biomass burning in Amazonia, *Atmos. Chem. Phys.*, *5*, 2,989–3,002.

Heald, C. L., D. J. Jacob, D. B. A. Jones, P. I. Palmer, J. A. Logan, D. G. Streets, G. W. Sachse, J. C. Gille, R. N. Hoffman, and T. Nehrkorn (2004), Comparative inverse analysis of satellite (MOPITT) and aircraft (TRACE-P) observations to estimate Asian sources of carbon monoxide, *J. Geophys. Res.*, *109*, D23306, doi:10.1029/2004JD005185.

Ho, S.-P., D. P. Edwards, J. C. Gille, M. Luo, G. B. Osterman, S. S. Kulawik, and H. Worden (2009), A global comparison of carbon monoxide profiles and column amounts from Tropospheric Emission Spectrometer (TES) and Measurements of Pollution in the Troposphere (MOPITT), *J. Geophys. Res.*, *114*, D21307, doi:10.1029/2009JD012242.

Hooghiemstra, P. B., M. C. Krol, J. F. Meirink, P. Bergamaschi, G. R. van der Werf, P. C. Novelli, I. Aben, and T. Röckmann (2011), Optimizing global CO emissions using a four-dimensional variational data assimilation system and surface network observations, *Atmos. Chem. Phys. Discuss.*, *11*, 341–386.

Hooghiemstra, P. B., M. C. Krol, P. Bergamaschi, A. T. J. de Laat, G. R. van der Werf, P. C. Novelli, M. N. Deeter, I. Aben, and T. Röckmann (2012), Comparing optimized CO emission estimates using MOPITT or NOAA surface network observations, *J. Geophys. Res.*, *117*, D06309, doi:10.1029/2011JD017043.

Jacob, D. J., J. H. Crawford, M. M. Kleb, V. S. Connors, R. J. Bendura, J. L. Raper, G. W. Sachse, J. C. Gille, L. Emmons and C. L. Heald (2003), Transport and Chemical Evolution over the Pacific (TRACE-P) aircraft mission: Design, execution, and first results, *J. Geophys. Res.*, *108*(D20), 9000, doi:10.1029/2002JD003276.

Jiang, Z., D. B. A. Jones, M. Kopacz, J. Liu, D. K. Henze, and C. Heald (2011), Quantifying the impact of model errors on top-down estimates of carbon monoxide emissions using satellite observations, *J. Geophys. Res.*, *116*, D15306, doi:10.1029/2010JD015282.

Jiang, Z., D. B. A. Jones, H. M. Worden, M. N. Deeter, D. K. Henze, J. Worden, K. W. Bowman, C. A. M. Brenninkmeijer, and T. J. Schuck (2013), Impact of model errors in convective transport on CO source estimates inferred from MOPITT CO retrievals, *J. Geophys. Res. Atmos.*, *118*, 2,073–2,083, doi:10.1002/jgrd.50216.

Jones, D. B. A., K. W. Bowman, P. I. Palmer, J. R. Worden, D. J. Jacob, R. N. Hoffman, I. Bey, and R. M. Yantosca (2003) Potential of observations from the Tropospheric Emission Spectrometer to constrain continental sources of carbon monoxide, *J. Geophys. Res.*, *108*(D24), 4789, doi:10.1029/2003JD003702.

Jones, D. B. A., K. W. Bowman, J. A. Logan, C. L. Heald, J. Liu, M. Luo, J. Worden, and J. Drummond (2009), The zonal structure of tropical O3 and CO as observed by the Tropospheric Emission Spectrometer in November 2004 – Part 1: Inverse modeling of CO emissions, *Atmos. Chem. Phys.*, *9*, 3,547–3,562.

Kopacz, M., D. J. Jacob, D. K. Henze, C. L. Heald, D. G. Streets, and Q. Zhang (2009), Comparison of adjoint and analytical Bayesian inversion methods for constraining Asian sources of carbon monoxide using satellite (MOPITT) measurements of CO columns, *J. Geophys. Res.*, *114*, D04305, doi:10.1029/2007JD009264.

Kopacz, M., D. J. Jacob, J. A. Fisher, J. A. Logan, L. Zhang, I. A. Megretskaia, et al. (2010), Global estimates of CO sources with high resolution by adjoint inversion of multiple satellite datasets (MOPITT, AIRS, SCIAMACHY, TES), *Atmos. Chem. Phys.*, *10*, 855–876, doi:10.5194/acp-10-855-2010.

Li, F., X. D. Zeng, and S. Levis (2012), A process-based fire parameterization of intermediate complexity in a Dynamic Global Vegetation Model, *Biogeosciences Discuss.*, *9*, 3,233–3,287, doi:10.5194/bgd-9-3233-2012.

Lopez, J. P., M. Luo, L. E. Christensen, M. Loewenstein, H. Jost, C. R. Webster, and G. Osterman (2008), TES carbon monoxide validation during two AVE campaigns using the Argus and ALIAS instruments on NASA's WB-57F, *J. Geophys. Res.*, *113*, D16S47, doi:10.1029/2007JD008811.

Luo, M., et al. (2007), Comparison of carbon monoxide measurements by TES and MOPITT: Influence of a priori data and instrument characteristics on nadir atmospheric species retrievals, *J. Geophys. Res.*, *112*, D09303, doi:10.1029/2006JD007663.

Müller, J.-F., and T. Stavrakou (2005), Inversion of CO and NO_x emissions using the adjoint of the IMAGES model, *Atmos. Chem. Phys.*, *5*, 1,157–1,186, doi:10.5194/acp-5-1157-2005.

Pechony, O., and D. T. Shindell (2009), Fire parameterization on a global scale, *J. Geophys. Res.*, *114*, D16115, doi:10.1029/2009JD011927.

Pétron, G., et al. (2002), Inverse modeling of carbon monoxide surface emissions using CMDL network observations, *J. Geophys. Res.*, *107*(D24), 4761, doi:10.1029/2001JD001305.

Rodgers, C. D. (2000), *Inverse Methods for Atmospheric Sounding: Theory and Practice*, World Sci, Hackensack, N. J.

Schmidt, G. A. et al. (2006), Present day atmospheric simulations using GISS ModelE: Comparison to in-situ, satellite and reanalysis data, *J. Clim.*, *19*, 153–192.

Shindell, D. T., et al. (2006), Multimodel simulations of carbon monoxide: Comparison with observations and projected near-future changes, *J. Geophys. Res.*, *111*, D08302, doi:10.1029/2006JD007100.

Shindell, D. T., et al. (2013), Interactive ozone and methane chemistry in GISS-E2 historical and future climate simulations, *Atmos. Chem. Phys.*, *13*, 2,653–2,689, doi:10.5194/acp-13-2653-2013.

Stavrakou, T., and J.-F. Müller (2006), Grid-based versus big region approach for inverting CO emissions using Measurement of Pollution in the Troposphere (MOPITT) data, *J. Geophys. Res.*, *111*, D15304, doi:10.1029/2005JD006896.

Tost, H., M. G. Lawrence, C. Brühl, P. Jöckel, The GABRIEL Team, and The SCOUT-O3-DARWIN/ACTIVE Team (2010), Uncertainties in atmospheric chemistry modelling due to convection parameterisations and subsequent scavenging, *Atmos. Chem. Phys.*, *10*, 1,931–1,951.

Van der Werf, G. R., J. T. Randerson, L. Giglio, G. J. Collatz, P. S. Kasibhatla, and A. F. Jr.Arellano (2006), Interannual variability in global biomass burning emissions from 1997 to 2004, *Atmos. Chem. Phys.*, *6*, 3,423–3,441, doi:10.5194/acp-6-3423-2006.

Van der Werf, G. R., J. T. Randerson, L. Giglio, G. J. Collatz, M. Mu, P. S. Kasibhatla, D. C. Morton, R. S. DeFries, Y. Jin, and T. T. van Leeuwen (2010), Global fire emissions and the contribution of deforestation, savanna, forest, agricultural, and peat fires (1997–2009), *Atmos. Chem. Phys.*, *10*, 11,707–11,735, doi:10.5194/acp-10-11707-2010.

Worden, J., S. Sund-Kulawik, M. W. Shephard, S. A. Clough, H. Worden, K. Bowman, A. Goldman (2004) Predicted errors of tropospheric emission spectrometer nadir retrievals from spectral window selection, *J. Geophys. Res.*, *109*(D9), D09308 doi:10.1029/2004JD004522.

Worden, H. M., M. N. Deeter, D. P. Edwards, J. C. Gille, J. R. Drummond, and P. Nédélec (2010), Observations of near-surface carbon monoxide from space using MOPITT multispectral retrievals, *J. Geophys. Res.*, *115*, D18314, doi:10.1029/2010JD014242.

Zhang, L., et al. (2008), Transpacific transport of ozone pollution and the effect of recent Asian emission increases on air quality in North America: An integrated analysis using satellite, aircraft, ozonesonde, and surface observations, *Atmos. Chem. Phys.*, *8*, 6,117–6,136, doi:10.5194/acp-8-6117-2008.